energies

MDPI

Article

Surrogate Model-Based Heat Sink Design for Energy Storage Converters

Gege Qiao [1], Wenping Cao [1,*], Yawei Hu [1], Jiucheng Li [2], Lu Sun [2] and Cungang Hu [1]

[1] School of Electrical Engineering and Automation, Anhui University, Hefei 230031, China
[2] Asunx Semiconductors Co., Ltd., Hefei 230093, China
* Correspondence: wpcao@ahu.edu.cn

Abstract: As forced-air cooling for heat sinks is widely used in the cooling design of electrical and electronic equipment, their thermal performance is of critical importance for maintaining excellent cooling capacity while reducing the size and weight of the heat sink and the equipment as a whole. This paper presents a method based on the combination of computational fluid dynamics (CFD) simulation and surrogate models to optimize heat sinks for high-end energy storage converters. The design takes the thermal resistance and mass of the heat sink as the optimization goals and looks for the best design for the fin height, thickness and spacing, as well as the base thickness. The analytical and numerical results show that the thermal resistance and mass of the heat sink are reduced by the proposed algorithms, as are the temperatures of the heating elements. Test results verify the effectiveness of the optimization method combining CFD simulation with surrogate models.

Keywords: computational fluid dynamics (CFD); energy storage; surrogate model; design optimization; heat sinks; power converters

Citation: Qiao, G.; Cao, W.; Hu, Y.; Li, J.; Sun, L.; Hu, C. Surrogate Model-Based Heat Sink Design for Energy Storage Converters. *Energies* **2023**, *16*, 1075. https://doi.org/10.3390/en16031075

Academic Editor: Alon Kuperman

Received: 31 October 2022
Revised: 30 November 2022
Accepted: 8 December 2022
Published: 18 January 2023

1. Introduction

In the face of global warming and the rapid depletion of fossil-fuel resources, the utilization of renewable energy has become a general trend across the world. With the large-scale and high penetration of renewable energy in power grids, the stable supply of electricity and energy-storage technologies have become technical concerns. Power Conversion Systems (PCS) can improve the utilization quality of clean energy and stabilize the load fluctuations of the power grid. In some cases, PCS can be used as an energy source where power grids are not available (i.e., power islands). Because of these advantages, PCS are gaining in popularity in industrial, as well as domestic, applications. In PCS power electronics converters, switching devices such as metal-oxide-semiconductor field-effect transistors (MOSFETs) and insulated gate bipolar transistors (IGBTs) are major heat sources and the heat is removed typically by heat sinks, which can be of natural cooling or forced-air cooling. The thermal performance of components such as IGBTs is directly related to the reliability of the whole converter. Recognizing that the main cause of electronic equipment failure is overheating [1], heat sink design for converters is a key focus of this work.

In the literature, quantitative analysis of the key parameters is considered useful. Typically, the analysis is based on calculating the thermal resistance of the heat sink, which is related to the thickness of the substrate, and the number and thickness of the heat sink fins. However, this does not give an optimization method for the structural design of the heat sink [2]. In some cases, the geometric parameters that affect the thermal resistance of the heat sink are optimized by using a genetic algorithm method [3]. Ref. [4] studies the influence of a single parameter of the heat sink on the performance and then develops the orthogonal method to assess the influence of different parameters on the performance of the heat sink. However, the design cycle is tedious, and the experimental cost is relatively high. Generally, when studying the heat dissipation performance of a heat sink, it is necessary

to consider not only the thermal resistance but also the volume and the cost of the heat sink. There are several parameters that affect the heat dissipation performance of the heat sink, such as the thickness of the base, and the length, thickness and number of fins. The optimization in this paper considers the influence of multiple parameters for multiple optimization targets. In this paper, the heat sink and forced air cooling are used in an IGBT-based energy storage converter where IGBTs are considered the main heat sources for cooling design. CFD simulation and surrogate model algorithms are combined to realize the double objective optimization (the thermal resistance and mass of the heat sink). The optimal parameter design can be obtained by bringing the optimized results into the CFD model to verify the correctness of the designs.

2. Mathematical Model

This work carries out a thermal analysis of a high-end PCS converter which involves an extensive understanding of heat transfer within a heat sink.

2.1. Design Variables

In this work, there are four independent variables: the thickness of the base, and fin height, thickness and spacing. The structural diagram of the optimized forced-air-cooled heat sink is shown in Figure 1.

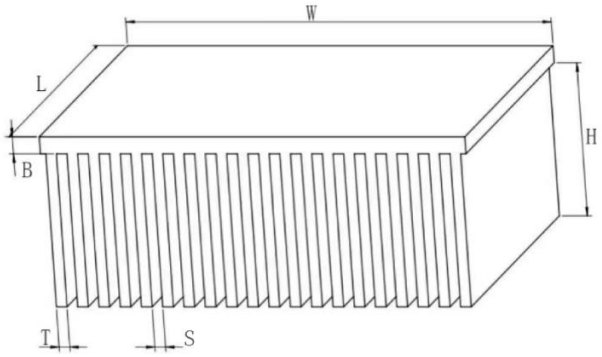

Figure 1. Structural diagram of the forced-air-cooled heat sink.

Where B is the thickness of the base, and H, T and X are the height, thickness and spacing of the fins, respectively, all of which taken together are defined as x_1, x_2, x_3, x_4, W is the width of the heat sink, L is the length of the heat sink and H is the height of the heat sink. Based on these variables, the thermal resistance and mass of the heat sink can be obtained and used as the objective functions of the optimization design.

2.1.1. Boundary Conditions

The optimization variables of the heat sink are associated with IGBT size, fan size, model and airflow rate. For effective heat transfer, the height of the fins shall not be greater than that of the fan, otherwise, airflow misses part of the fins and reduces the heat dissipation performance. Similarly, the spacing between fins shall be greater than 1 mm. The thickness of the heat sink fin shall be greater than 1 mm for easy manufacture. In summary, the constraints of design optimization are given by:

$$\begin{cases} 1\text{mm} \leq x_1 \leq 20\text{mm} \\ 50\text{mm} \leq x_2 \leq 100\text{mm} \\ 1\text{mm} \leq x_3 \leq 4\text{mm} \\ 1\text{mm} \leq x_4 \leq 8\text{mm} \end{cases} \quad (1)$$

2.1.2. Objective Functions

Considering the heat dissipation in the heat sink, the optimization objectives of the heat sink are low thermal resistance, low mass, high heat transfer efficiency and overall

cost. In this paper, the thermal resistance and mass of the heat sink are selected as the design targets, and the entropy weight method [5] and linear weighting method [6] are combined to process the numerical data. This processing method can not only solve the problem of different variable units but also eliminate the influence of different variable values on the optimization results, making the data dimensionless for comparison [7]. The specific process of data processing has five steps:

- Standardize the data;

$$T_{ij} = \frac{\max(x_{1j}, \ldots, x_{nj}) - x_{ij}}{\max(x_{1j}, \ldots, x_{nj}) - \min(x_{1j}, \ldots, x_{nj})} + 0.0001 \quad (2)$$

- Calculate the entropy value of the jth index, which ranges between 0 and 1;

$$e_j = -\left(\frac{1}{\ln n}\right)\sum_{i=1}^{n} \frac{T_{ij}}{\sum_{i=1}^{n} T_{ij}} \ln \frac{T_{ij}}{\sum_{i=1}^{n} T_{ij}} \quad (3)$$

- Calculate the weighting of each data set (I = 1,2 . . . ,n; j = 1,2 . . . ,m);

$$w_j = \frac{1 - e_j}{\sum_{j=1}^{m} (1 - e_j)} \quad (4)$$

- Establish the priority function of the targets, based on the linear weighting method;

$$P_i = \sum_{j=1}^{m} w_j x_{ij} \quad (5)$$

- Obtain the multi-objective optimization function of the heat sink;

$$\min F(x) = \min[w_1 R(x) + w_2 M(x)] \quad (6)$$

From the above calculations, the weightings of the thermal resistance and the mass are:

$$w_1 = 0.588,$$
$$w_2 = 0.412.$$

2.2. Thermal Resistance Model

The thermal resistance of the heat sink consists of four parts [8], the thermal resistance between the junction and the device case, the thermal resistance between the shell and the environment, the thermal resistance between the shell and the heat sink, and the thermal resistance between the heat sink and the environment [9]. Figure 2 shows the equivalent thermal resistance network diagram of the heat sink.

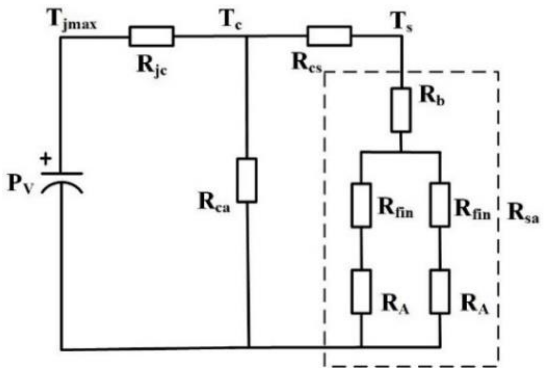

Figure 2. Thermal resistance model.

In Figure 2, P_V is the total heat loss of the IGBT, R_{jc} is the thermal resistance between the junction and shell, R_{ca} is the thermal resistance between the shell and the environment, R_{cs} is the thermal resistance between the shell and heat sink and R_{sa} and is the thermal resistance between the heat sink and the environment. R_b is the heat conduction resistance of the heat sink base, R_{fin} is the heat conduction resistance of the fins and R_A is the heat convection resistance of the fins. Similar to electrical resistances in electrical circuits, the thermal resistance can be calculated by adding up the component resistances according to their series or parallel connections. The heat transfer in the forced-air-cooled heat sink follows Ohm's law for thermal circuits. Compared with R_{cs} and R_{sa}, R_{ca} is very large and can be ignored in parallel connection; then:

$$\Delta T = P\left(R_{jc} + R_{cs} + R_{sa}\right) \tag{7}$$

According to Equation (7), the temperature rise of the device is determined by the loss and thermal resistance of the power device. The losses of power devices and the thermal resistance of the junction–shell are mainly determined by the production process, packaging materials and performance index. These two parameters are constant values [10]. The thermal resistance between the shell and heat sink is very small and can be ignored. The thermal resistance between the heat sink and the environment can be reduced by optimizing the geometric structure, materials and external environment of the heat sink. Compared to other parameters, the thermal resistance between the heat sink and the environment is also relatively simple and convenient to optimize. For this reason, the thermal resistance between the heat sink and the environment is the objective that majorly corresponds to the total thermal resistance.

2.3. Optimization Model

The thermal resistance of the heat sink in this design is mainly composed of the heat convection thermal resistance and the heat conduction resistance of the heat sink base and fins, which can be calculated by Equations (8)–(10). The total thermal resistance of the heat sink can be calculated by Equation (11).

$$R_b = \frac{B}{k_s WL} \tag{8}$$

$$R_{fin} = \frac{H}{k_s TL} \tag{9}$$

$$R_A = \frac{1 - 0.152(vL)^{-\frac{1}{10}}}{5.12(vL)^{\frac{4}{5}}(H+S)\cdot 2N} \tag{10}$$

$$R_{sa} = R_b + \frac{R_{fin}}{2N} + R_A \tag{11}$$

where N is the number of air ducts, ks is the thermal conductivity of the heat sink material and v is the airflow velocity.

In this design, the size of the heat sink is 230 × 420 mm and the height is variable. According to Equations (8)–(11), the optimization model of the heat sink resistance is:

$$\min F_1 = \frac{x_1}{k_s * 420 * 230} + \frac{x_2}{k_s * x_3 * 230}8 + \frac{1 - 0.152(230v)^{-\frac{1}{10}}}{5.12(230v)^{\frac{4}{5}}(x_2 + x_4) * 2 * \left\{\left[\frac{420 - x_3}{x_3 + x_4}\right] + 1\right\}} \tag{12}$$

From Figure 2, the heat sink mass optimization model is:

$$\min F_2 = 420 * 230 * x_1\rho_m + 230 * x_2x_3x_5\rho_m \tag{13}$$

where ρ_m is the density of the heat sink material, which is aluminum in this case.

3. The Proposed Optimization Methods

In the literature, surrogate model algorithms are adopted, which do not rely on actual models, thus reducing computational time and cost. The surrogate model algorithms use a Kriging algorithm to establish a simplified model by using basic parameters such as independent variables, objective functions and limiting conditions [11]. The success of the surrogate model depends on its sampling strategy and the number and location of sampling points [12]. The generated sample points should accurately reflect the distribution characteristics of sampling points [13,14]. A Kriging algorithm is then applied to search for the optimization point.

3.1. Kriging Models

At present, the methods of establishing models are divided into two categories: one is a parametric model, and the other is a non-parametric model. The former is based on the assumption that the known parameters obey a given population distribution. The latter model does not assume any particular distribution of the population. In the case of a given sample, it is calculated according to non-parametric statistics [15].

In the optimization, a Kriging model based on a parametric model is selected, which is also an alternative model widely used at present. The Kriging model is given by [16–18]:

$$y(x) = \mu + z(x) \tag{14}$$

where $y(x)$ is the response function, μ is the constant, $z(x)$ is the random process, respectively. Its expectation, variance and covariance are:

$$\begin{cases} E[z(x)] = 0 \\ Var[z(x)] = \sigma^2 \\ cov[z(x^j), z(x^k)] = \sigma^2 R[R(x^j, x^k)] \end{cases} \tag{15}$$

where R is the symmetric correlation matrix on the diagonal, $R(x^i, x^j)$ and is the correlation parameter between sample points x^j, x^k. In this optimization, a Gaussian correlation function is selected, then

$$R(x^j, x^k) = \exp[-\sum_{i=1}^{n} \theta_i \left| x_i^j - x_i^k \right|^2] \tag{16}$$

where n is the number of groups of design variables. In this optimization, $n = 50$. $\left| x_i^j - x_i^k \right|$ is the distance between the kth components of sample points x^j and x^k, and θ_i is the unknown related parameter used to fit the model, which can be solved by Equation (17).

$$\max F(\theta_i) = -\frac{[n_s \ln(\widehat{\sigma}^2) + \ln|R|]}{2} \tag{17}$$

Then, the estimated value at sample point x is:

$$\widehat{y}(x) = \widehat{\mu} + r^T(x) R^{-1}(y - \widehat{\mu} m) \tag{18}$$

$$r^T(x) = [R(x, x^1), R(x, x^2), \ldots R(x, x^{n_s})]^T \tag{19}$$

where y is the column vector with length n_s and m is the unit vector.

Figure 3 shows six Kriging models constructed with different variables and target parameters. It can be seen that the Kriging models differ from their 2D parameters and objectives. Considering different two-dimensional parameters and the minimum value of the objective function, a set of optimization values can be generated. This design needs to consider that the target value is the lowest in the case of four-dimensional parameters, which requires a search algorithm to find the target minimum value [19].

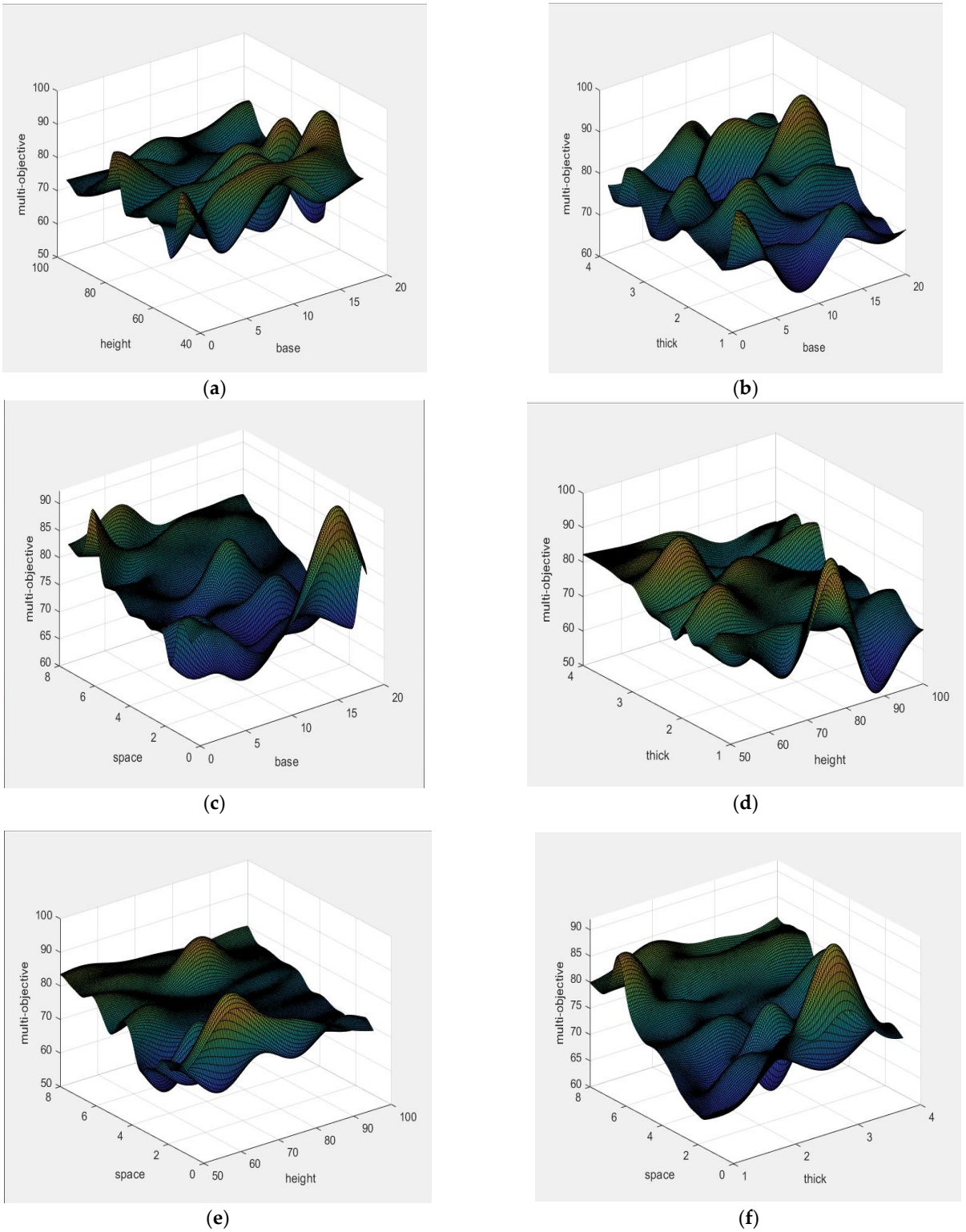

Figure 3. Kriging model constructed with different variables and target parameters. (**a**) Kriging model constructed with B, H and multi-objective. (**b**) Kriging model constructed with B, T and multi-objective. (**c**) Kriging model constructed with B, S and multi-objective. (**d**) Kriging model constructed with H, T and multi-objective. (**e**) Kriging model constructed with H, S and multi-objective. (**f**) Kriging model constructed with T, S and multi-objective.

3.2. Particle Swarm Optimization (PSO) Algorithm

In the literature, particle swarm optimization (PSO) algorithms are favored due to their advantages of easy programming, high efficiency and fast convergence [20], the optimization in this paper selects PSO as the search algorithm. Each particle in the particle swarm itself can find the optimal solution of its current position and record it as an individual extreme value. Particles can share an individual extremum with other particles, and the optimal individual extremum is regarded as the global optimal solution of the whole particle swarm [21]. Then, the particle adjusts its speed and position according to its individual extreme value and the current global optimal solution, and constantly approaches the optimal solution [22]. The PSO algorithm is shown in Equation (20).

$$\begin{cases} V_i^{k+1} = wV_i^k + C_1r_1(P_i^k - X_i^k) + C_2r_2(P_g^k - X_i^k) \\ X_i^{k+1} = X_i^k + V_i^{k+1} \end{cases} \tag{20}$$

where V_i^k and X_i^k are the velocity and position of the ith particle at the kth iteration, P_i^k represents the individual extreme value of the ith particle at the kth iteration, P_g^k represents the global optimal solution of the ith particle at the kth iteration, C_1 and C_2 are individual learning factors and global learning factors of particles, r_1 and r_2 are random constants between $[0, 1]$ and w is the inertia weight, respectively. In this design, the value of w decreases linearly according to the number of iterations k. The equation is given by [23]:

$$w(k) = w_{max} - \frac{w_{max} - w_{min}}{k_{max}} \times k \tag{21}$$

where w_{max}, w_{min} are the upper and lower limits of the inertia weight and k_{max} is the maximum number of iterations, respectively.

3.3. Process of Surrogate Algorithms

The whole optimization process is shown in Figure 4. First, design the variables and determine the range of independent variables, and then take Latin hypercube sampling [24]. After obtaining a limited number of sample points, choose whether to supplement points in some areas or redesign the design according to the sampling conditions of the sample points [25]. The sampling condition of this design is good, so the supplement of sample points is not considered. The second step is the selection of target parameters. This can choose single objective optimization or multi-objective optimization according to the design requirements. In general, the objectives of multi-objective optimization are in conflict with each other. The improvement of one sub-objective may cause the reduction of another sub-objective, and the solution result cannot make all sub-objectives optimal. This requires that, when carrying out multi-objective optimization, the weight proportion between different objectives should be considered [26]. In the multi-objective optimization problem, the solution is not unique, which requires specific analysis of specific problems in the optimization design to find solutions that meet more sub-objectives as much as possible. In this process, the optimal design should meet the requirements of independent variables, constraints and target parameters at the same time. The third step is to establish a finite element model and use the finite element model to obtain relevant parameters. Then, the Kriging model is established using 80% of the sampled data for an approximate model, which is used to replace the established finite element model. The remaining 20% is used for error detection. If the error between the data obtained from the approximate model and the simulation is within the 20% threshold, the surrogate model is considered successful. After error detection, the PSO algorithm is used to obtain the optimal solution, which is finally brought into the finite element model to verify the results, to complete the optimization design [27].

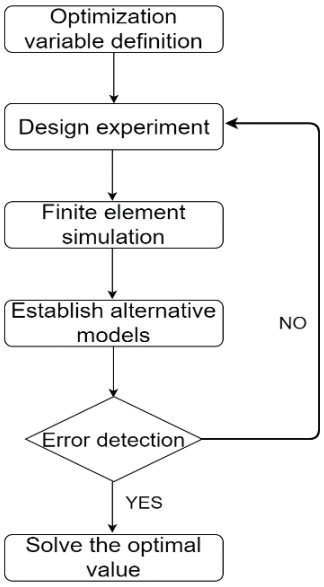

Figure 4. Flowchart of the process of surrogate algorithms.

4. Simulation Results

The structure of the PCS converter is complex for 3D thermal modeling and analysis. In this work, a simplified model is developed for design optimization, and the 3D finite element model only includes key components, as shown in Figure 5.

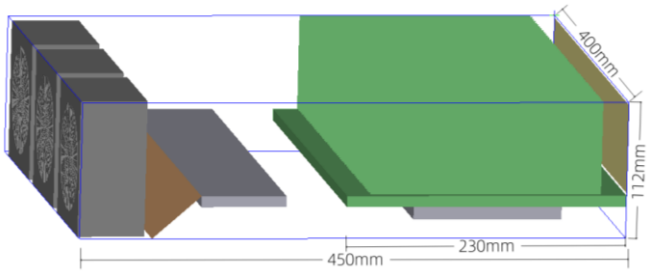

Figure 5. 3D finite element model.

In this converter, four heating element IGBTs are installed on the base of the heat sink, and the three fans blow air to the fins of the heat sink through the air deflector. In the model, the size of the cabinet is 450 mm × 400 mm × 114 mm, the radius of the fan is 44 mm, the size of the IGBT is 122 mm × 62 mm × 14 mm, and the spacing between IGBTs is 38 mm. The length and width of the heat sink base are 420 mm and 230 mm, the height of the base is 12 mm, the height and thickness of the fins are 64 mm and 3.4 mm, and the spacing between heat sinks is 7 mm, respectively. The power loss of each IGBT is 800 W, and the total power loss is 3200 W. The ambient temperature is 50 °C. The simulation results are plotted in Figures 6–9. It can be seen that the maximum temperature of the heating element can reach 133.43 °C. The calculated results are brought into the finite element model for verification. The finite element simulation and optimization results are shown in Figures 6–9, respectively.

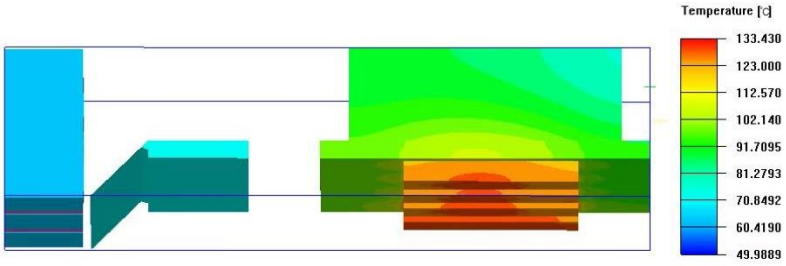

Figure 6. 3D Finite element simulation results before optimization.

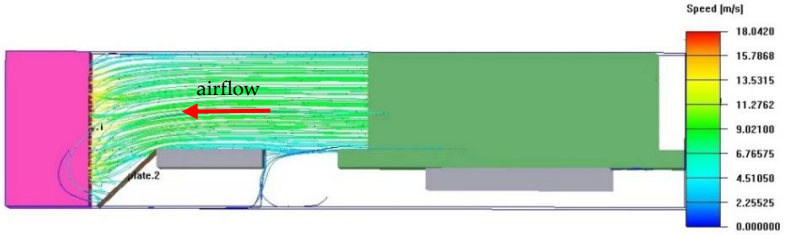

Figure 7. Airflow speed vector results before optimization.

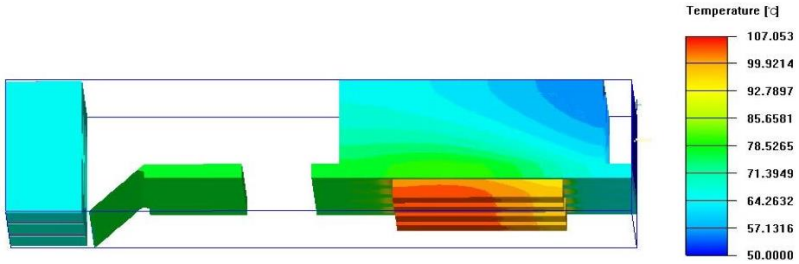

Figure 8. 3D Finite element simulation results after optimization.

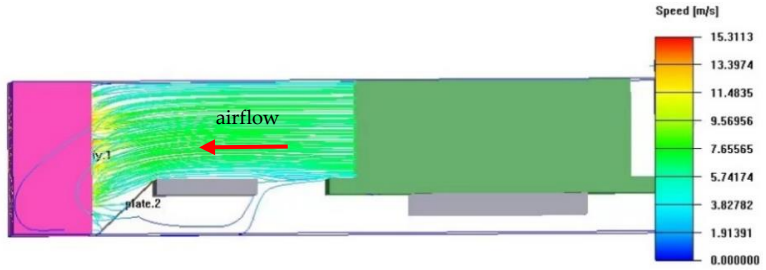

Figure 9. Airflow speed vector results after optimization.

It can be seen that the maximum airflow velocity after optimization is significantly reduced. The changes in the heat sink ducts and the relative positions of the heat sink and fans can vary the airflow path and contact surface of the heatsink, which is confirmed by Figures 6 and 8.

In contrast, a traditional method with response surface optimization in ANSYS adopts an optimization algorithm, as illustrated in Table 1. The proposed surrogate optimization results with the surrogate model are better. After the optimization design, the thermal resistance and mass are reduced from 0.025 °C/W and 7.562 kg to 0.017 °C/W and 7.312 kg, respectively. From the temperature cloud diagrams in the 3D finite element simulation, it can also be seen that the hot-spot temperature is reduced from the 133.430 °C value to 107.053 °C, proving the effectiveness of the proposed surrogate optimization algorithms.

Table 1. Optimum design of the heat sink.

	B	H	T	S	Thermal	Mass	Temperature
Base design	12.0 mm	64.0 mm	3.4 mm	7.0 mm	0.0253 °C/W	7.562 kg	133.430 °C
Traditional design	8.0 mm	80.0 mm	2.0 mm	4.4 mm	0.0194 °C/W	7.423 kg	114.733 °C
Optimization design	10.8 mm	65.6 mm	1.1 mm	2.3 mm	0.0171 °C/W	7.312 kg	107.053 °C
Reduction (%)	10.0	−2.5	67.6	67.1	32.4	3.3	19.8

5. Gray Correlation Analysis

Gray correlation analysis can evaluate the importance of input parameters, calculate the impact of different parameters on multiple objectives, and verify the selection of parameters in the design [28]. After all data are made dimensionless [29], the correlation coefficient is calculated by Equation (22). Then the average value is calculated to obtain the gray correlation degree of each parameter with the target [30].

$$\begin{cases} r_i^k = \frac{\Delta_{min} + \lambda\Delta_{max}}{\Delta_i^k + \lambda\Delta_{max}} \\ \Delta_i^k = |y_0^k - y_i^k| \end{cases} \quad (22)$$

where r_i^k represents the correlation coefficient of the kth component of the ith parameter, y_0^k and y_i^k represents the results of dimensionless processing of the reference sequence and the comparison sequence, Δ_i^k represents the deviation sequence, Δ_{min} and Δ_{max} represents the minimum and maximum deviation, and λ is the resolution coefficient, respectively. In this design, the resolution coefficient is taken as 0.5. The gray correlation degrees of the four variables relative to thermal resistance, mass and weighted multi-objective are shown in Table 2.

Table 2. Summary of Gray correlation analysis.

Dimensionless	Base	Height	Thick	Space
Temperature	0.637699	0.590268	0.668855	0.697728
Mass	0.622044	0.673455	0.698375	0.605095
Multi-objective	0.639337	0.586499	0.672616	0.726296

Within the given range of variables, the four design variables have a high degree of correlation with the target parameters, and the correlation degree can basically reach 0.6, which also proves the rationality of the design variables selected. Of these, for the temperature single target, the spacing of the heat sink fins has the greatest influence, and the correlation degree is as high as 0.7. The correlation degree of the thickness of the fins is the second, which is 0.67. Compared with other parameters, the correlation between the thickness of the fins and the temperature is the smallest, but it can also reach 0.59. It can also be seen that the airflow path is very crucial for the heat dissipation optimization design, while the influence of the surface area of the fins is less obvious. For the mass in the target parameters, the parameter with the greatest correlation is the thickness of the fins, and the correlation reaches 0.7. For the dual objectives of thermal resistance and mass, the most relevant parameter in this optimization is fin spacing, which is as high as 0.73, and the second important parameter is fin thickness, with a correlation degree of 0.67. By comparison, fin height has the smallest correlation degree with the double targets, with a correlation coefficient of 0.59. In this double objective optimization, fin spacing and thickness are the most significant factors affecting the performance of the heat sink.

6. Conclusions

This paper has presented an optimization method for heat sinks based on the CFD method and surrogate models. Firstly, the heat dissipation process is simulated by using the 3D finite element model. Next, using the sampling points selected by Latin hypercube

sampling and the simulation results of CFD, a surrogate model is established to assess the correlation of four design variables (B, H, T, S) and the two design targets (thermal resistance and mass), according to Kriging models. Then a PSO algorithm is used to obtain the optimal solution. The test results show that the optimized thickness of the base and the height, thickness and spacing of the fins can effectively reduce the thermal resistance of the heat sink and the mass of the heat sink. In turn, the proposed method can reduce hotspots (such as an IGBT junction) and improve the thermal efficiency of the converters. The developed technology can provide guidance for heat sink designs and optimize the energy efficiency of industrial products.

Author Contributions: Conceptualization, J.L. and Y.H.; methodology, W.C.; software, G.Q.; validation, G.Q., Y.H. and J.L.; investigation, C.H.; resources, L.S.; writing—original draft preparation, G.Q.; writing—review and editing, W.C.; supervision, C.H.; project administration, L.S.; funding acquisition, W.C. All authors have read and agreed to the published version of the manuscript.

Funding: This research received no external funding.

Institutional Review Board Statement: Not applicable.

Informed Consent Statement: Not applicable.

Data Availability Statement: Not applicable.

Conflicts of Interest: The authors declare no conflict of interest.

References

1. Shen, L.; Jiang, J.; Fang, Y.; Yang, Z.; Hou, Y. Design and optimization of IGBT heat dissipation scheme based on air cooling. *Refrigeration* **2018**, *46*, 95–98. Available online: https://kns.cnki.net/kcms/detail/detail.aspx?dbcode=CJFD&dbname=CJFDLAST2018&filename=DWYC201808019&uniplatform=NZKPT&v=nUx0m-QPZhytRoXds8TOiuHzmCdP5uH1I_Uzb7RhTEH_qRCRtFADpE4g2Y3YYuAG (accessed on 2 October 2022).
2. Zhao, H.; Zhu, Y.; Yin, Z. Thermal design of high-power inverter. *Electr. Eng.* **2018**, *19*, 149–156. Available online: https://kns.cnki.net/kcms/detail/detail.aspx?dbcode=CJFD&dbname=CJFDLAST2018&filename=DQJS201808038&uniplatform=NZKPT&v=n_mEH02HHLKWCbqbWeO9nd-3v3886CNvSUdQOT5OKvevOzmFThtUhOHsl5EupxBP (accessed on 2 October 2022).
3. Zhou, Z.; Bing, L.; Jian, L.; Wan, Y.; Du, L.; Chao, W. Optimization design of heat sink fins based on genetic algorithm. *Electro-Mech. Eng.* **2019**, *35*, 29–33. Available online: https://kns.cnki.net/kcms/detail/detail.aspx?dbcode=CJFD&dbname=CJFDLAST2019&filename=DZJX201905008&uniplatform=NZKPT&v=nt8dGV7hmt5S8ncV0n3---hVbYTvtRD2CAAPp6_QE1vOV-oE9SnpMWDTccGxpbl8 (accessed on 2 October 2022).
4. Ding, C.; Zhang, T.; Luo, J.; Cui, Y.; Yu, L. Optimization design research on high power LED lamps of radiator. *Chin. J. Electron Device* **2016**, *39*, 750–754. Available online: https://kns.cnki.net/kcms/detail/detail.aspx?dbcode=CJFD&dbname=CJFDLAST2016&filename=DZQJ201603049&uniplatform=NZKPT&v=sT7RuFw0Jcb0cMM5ZwdbJG9TvAVwhHAs5PcbCqqzrv7fmyTxGBmNqIA3EtFPazCn (accessed on 2 October 2022).
5. Zhang, M.; Du, J.; Luo, J.; Nie, B.; Xiong, W.; Liu, M.; Zhao, S. Research on feature selection of multi-objective optimization. Available online: https://kns.cnki.net/kcms/detail/detail.aspx?dbcode=CAPJ&dbname=CAPJLAST&filename=JSGG20221020002&uniplatform=NZKPT&v=ZhiUyUsnOHCdm5VBxZlxys-l7vytq9hLD_NRIC7eFcufvCP13qxIm0EIE2mu6c1- (accessed on 2 October 2022).
6. Li, J.; Yang, Q.; Niu, P.; Xian, Z.; Zhang, J.; Liang, J.; Li, Y. Optimization design and analysis of high-power LED heat radiator based on genetic algorithm and matlab simulation. *Trans. China Electrotech. Soc.* **2013**, *28*, 213–220.
7. Zhao, J.; Zhang, M.; Zhu, Y.; Cheng, R.; Li, X.; Wang, L.; Hu, C. Thermofluid modeling for concurrent size-topology optimization of heat sinks for planar motors. *J. Tsinghua Univ. (Sci. Technol.)* **2022**, *62*, 400–407.
8. Wang, L.; Li, L.; Zhou, X.; Zhu, S.; Sun, C. Multi-objective optimization of forced air-cooled heatsink based on particle swarm optimization algorithm. *Electr. Eng.* **2022**, *23*, 20–25. Available online: https://kns.cnki.net/kcms/detail/detail.aspx?dbcode=CJFD&dbname=CJFDLAST2022&filename=DQJS202202004&uniplatform=NZKPT&v=8V4xD_7-9NRAGCJQNf7AZZNJ0KrFU2GHCrBqHXQ71FF7V1e4gGBdMwh10_NeK_w4 (accessed on 2 October 2022).
9. Zhou, Z.; Li, X.; Wang, S.; Yin, F.; Lu, Y.; Xin, L.; Wang, L.C. Optimal design of heat sink for CLLLC resonant converter. *J. Power Sources* **2021**, *45*, 382–385. Available online: https://kns.cnki.net/kcms/detail/detail.aspx?dbcode=CJFD&dbname=CJFDLAST2021&filename=DYJS202103030&uniplatform=NZKPT&v=AktyuqzNqLsb8YPYZs74uvICbCqugPQ35skddfKV4NqOAVoQp1KffrFdyq9QoCoM (accessed on 2 October 2022).
10. Lu, X.; Xie, L.; Hou, W.; Ling, Xie; Wen, Hou. Two-Stage Operational Amplifier Based on Multipath Zero Point Elimination. *Ind. Technol. Innov.* **2020**, *7*, 45–49. Available online: https://kns.cnki.net/kcms2/article/abstract?v=3uoqIhG8C44YLTlOAiTRKibYlV5Vjs7iy_Rpms2pqwbFRRUtoUImHW0PuUQKlilXd9Fxpb85H68pH_Sw3R_1vgsyRoGwC-cm&uniplatform=NZKPT (accessed on 2 October 2022).

11. Hu, G.; Chen, Z.; Zhang, D. Optimization design of diaphragm profile based on Kriging model. *J. Mech. Transm.* **2022**, *46*, 75–79. Available online: https://kns.cnki.net/kcms2/article/abstract?v=3uoqIhG8C44YLTlOAiTRKibYlV5Vjs7iJTKGjg9uTdeTsOI_ra5_Xceslx1ry8096OvZ5q1IbQBEzsn1ubniRA27XgbxfeFA&uniplatform=NZKPT (accessed on 2 October 2022).
12. Cai, D.; Shi, D.; Chen, J. Probabilistic load flow calculation method based on polynomial normal transformation and latin hypercube sampling. *Proc. CSEF* **2013**, *13*, 92–100. Available online: https://kns.cnki.net/kcms2/article/abstract?v=3uoqIhG8C44YLTlOAiTRKgchrJ08w1e7xAZywCwkEEK4n59o2U1FxvRsc3oI8uuQBUK6uJ_wVNHLPqnb-QWhlU-_a6KQ-7cA&uniplatform=NZKPT (accessed on 2 October 2022).
13. Shin, P.S.; Woo, S.H.; Zhang, Y.; Koh, C.S. An application of latin hypercube sampling strategy for cogging torque reduction of large-scale permanent magnet motor. *IEEE Trans. Magn.* **2008**, *44*, 4421–4424. Available online: https://ieeexplore.ieee.org/document/4717645 (accessed on 2 October 2022).
14. Zhang, Z.; Jiao, C.; Sang, T.; Zhang, Q. Latin Hypercube Sampling Simulation of Response Surface Model Parameters of vehicle body. *Comput. Simul.* **2021**, *38*, 123–127. Available online: https://kns.cnki.net/kcms2/article/abstract?v=3uoqIhG8C44YLTlOAiTRKibYlV5Vjs7iy_Rpms2pqwbFRRUtoUImHVM9wC0ZpO3S8Q-VDu0JUxw3LVKKDFLOhDjEy3_7mHLF&uniplatform=NZKPT (accessed on 2 October 2022).
15. Feng, X.; Hua, J.; Zhou, S.; Yin, Y.; Shuai, Z.; Wang, X. Optimal design for geological sedimentation simulation platform based on Kriging model. *China Sci.* **2022**, *17*, 1162–1166. Available online: https://kns.cnki.net/kcms2/article/abstract?v=3uoqIhG8C44YLTlOAiTRKibYlV5Vjs7iJTKGjg9uTdeTsOI_ra5_XQ2lBi0_44Jk9CGGM_nlUP6OELW1Fykmky4OWHFEjXG-&uniplatform=NZKPT (accessed on 2 October 2022).
16. Wang, H. Kriging parameter estimation algorithm based on combination optimization. *Comput. Mod.* **2021**, *9*, 51–56.
17. Wang, W.; Li, J.; Liu, G.; Wei, J.; Zhang, Z.; Cheng, M. Optimization design of drum brake stability based on kriging surrogate model. *J. Vib. Shock* **2021**, *40*, 134–138. Available online: https://kns.cnki.net/kcms2/article/abstract?v=3uoqIhG8C44YLTlOAiTRKibYlV5Vjs7iy_Rpms2pqwbFRRUtoUImHZQQ2VJjpVrs5jV9FUVCoDNKnd-ew0sODo7ZKVX-tdM1&uniplatform=NZKPT (accessed on 2 October 2022).
18. Le, C.; Ma, Y. Parallel surrogate-based Optimization algorithm based on kriging model using adaptive multi-phases strategy. *Comput. Integr. Manuf. Syst.* **2021**, *27*, 3227–3235. Available online: https://kns.cnki.net/kcms2/article/abstract?v=3uoqIhG8C44YLTlOAiTRKibYlV5Vjs7iy_Rpms2pqwbFRRUtoUImHSIxD9BZFa_VvmZUniUwZU95L3EmKuzmE-ddjJXTZJxe&uniplatform=NZKPT (accessed on 2 October 2022).
19. Wen, X.; Tian, F.; Xie, F. Calculation method of fuzzy reliability of structures. *Mod. Ind. Econ. Inf.* **2022**, *12*, 263–265. Available online: https://kns.cnki.net/kcms2/article/abstract?v=3uoqIhG8C44YLTlOAiTRKibYlV5Vjs7iJTKGjg9uTdeTsOI_ra5_Xa2GWI2tEmmEDoI4GOZ2hXLdMXakEw2EcU6soX7qBnfb&uniplatform=NZKPT (accessed on 2 October 2022).
20. Chen, Z.; Wang, Y.; Chen, L.; Li, X. Structural damage identification based on improved particle swarm optimization algorithm with learning factors. *J. North China Univ. Water Resour. Electr. Power (Nat. Sci. Ed.)* **2022**, *43*, 43–47. Available online: https://kns.cnki.net/kcms2/article/abstract?v=3uoqIhG8C44YLTlOAiTRKibYlV5Vjs7iJTKGjg9uTdeTsOI_ra5_XdQLk (accessed on 2 October 2022).
21. Wang, Y.; Guo, R.; Liu, R.; Cui, H. Optimum design of double layer shaped charge structure based on PSO and SVM. *J. Ordnance Equip. Eng.* **2022**, *43*, 244–249. Available online: https://kns.cnki.net/kcms2/article/abstract?v=3uoqIhG8C44YLTlOAiTRKibYlV5Vjs7iJTKGjg9uTdeTsOI_ra5_XVwcEBwpKqCwKy-c-_FsnnAtveDuQf9WiSOClozTILiF&uniplatform=NZKPT (accessed on 2 October 2022).
22. Yan, Q.; Dong, X.; Mu, J.; Ma, Y. Optimal configuration of energy storage in an active distribution network based on improved multi-objective particle swarm optimization. *Power Syst. Prot. Control* **2022**, *50*, 11–19. Available online: https://kns.cnki.net/kcms2/article/abstract?v=3uoqIhG8C44YLTlOAiTRKibYlV5Vjs7iJTKGjg9uTdeTsOI_ra5_XReFrJuhIC5K2PEyefb-Yt9GnpyagDFG6PBhIVNvujbV&uniplatform=NZKPT (accessed on 2 October 2022).
23. Guo, P.; Luo, X.; Wang, Y.; Bai, L.; Li, H. Identification of shaft centerline orbit for hydropower units based on particle swarm optimization and improved BP neural network. *Proc. CSEE* **2011**, *31*, 93–97. Available online: http://www.alljournals.cn/view_abstract.aspx?pcid=5B3AB970F71A803DEACDC0559115BFCF0A068CD97DD29835&cid=6CDB4E49EF88F71A&jid=828E9BBC945455BDDF9DA6953F5D0883&aid=CADBAE05CAAADCCAE2148AD3563EDAC8&yid=9377ED8094509821 (accessed on 2 October 2022).
24. Morrow, J.; Littler, T.; Song, X.; Tan, Z.; Cao, W.; Yang, N. Asymmetrical rotor design for a synchronous machine based on surrogate optimization algorithm. In Proceedings of the 8th IET International Conference on Power Electronics, Machines and Drives (PEMD 2016), Glasgow, UK, 19–21 April 2016.
25. Song, X.; Zhang, J.; Kang, S.; Ma, M.; Ji, B.; Cao, W.; Pickert, V. Surrogate-based analysis and optimization for the design of heat sinks with jet impingement. *J. North China Univ. Water Resour. Electr. Power (Nat. Sci. Ed.)* **2014**, *4*, 429–437. [CrossRef]
26. He, T.; Shao, M.; Bai, X.; Cao, Z.; Jie, Y.L.F.; Wen, X. Research on multi-objective optimization of production line based on genetic algorithm. *Manag. Informatiz.* **2022**, *11*, 177–182. Available online: https://kns.cnki.net/kcms2/article/abstract?v=3uoqIhG8C44YLTlOAiTRKibYlV5Vjs7iJTKGjg9uTdeTsOI_ra5_XZIsdaxgLxFIeQqdxmAxav3r4qvVJzHxqfNawSEaMrCa&uniplatform=NZKPT (accessed on 2 October 2022).
27. Tan, Z.; Song, X.; Cao, W.; Liu, Z.; Tong, Y. DFIG Machine Design for Maximizing Power Output Based on Surrogate Optimization Algorithm. *IEEE Trans. Energy Convers.* **2015**, *30*, 1154–1162. Available online: https://ieeexplore.ieee.org/document/7078905 (accessed on 2 October 2022). [CrossRef]

28. Marco, L.; Cristiano, N.; Antonio, B. Survey and sensitivity analysis of critical parameters in lithium-ion battery thermo-electrochemical modeling. *Electrochim. Acta* **2021**, *394*, 139098. Available online: https://www.sciencedirect.com/science/article/abs/pii/S0013468621013888 (accessed on 2 October 2022).
29. Li, H.; Huang, D.; Xiong, Z.; Li, X.; Zhang, Z. Structural optimization of extrusion die for TA1 internal thread tube based on grey correlation degree. *J. Plast. Eng.* **2022**, *29*, 56–63. Available online: https://kns.cnki.net/kcms2/article/abstract?v=3uoqIhG8C44YLTlOAiTRKibYlV5Vjs7iJTKGjg9uTdeTsOI_ra5_XXbrszYM6X6oN9lDKVGDfsL_i4pEEA3G06dDVyHjB95e&uniplatform=NZKPT (accessed on 2 October 2022).
30. Wang, P.; Wang, X.; Liu, Z.; Wang, H.; Fu, H. Optimization of process parameters of ultrasonic rolling extrusion based on grey correlation analysis method. *J. Plast. Eng.* **2022**, *29*, 36–43. Available online: https://kns.cnki.net/kcms2/article/abstract?v=3uoqIhG8C44YLTlOAiTRKibYlV5Vjs7iJTKGjg9uTdeTsOI_ra5_XXbrszYM6X6o1DqxaPSM2JBbjiTpJzWFNvFlbX5kneu3&uniplatform=NZKPT (accessed on 2 October 2022).